Inferring origin of mercury inclusions in quartz by multifractal analysis

T. Shibata[1,2], T. Maruoka[3], and T. Echigo[4]

[1]{Geological Survey of Hokkaido, Hokkaido Research Organization, N19 W12, Kita-ku, Sapporo, Hokkaido 060-0819, Japan}

[2]{Institute for Geothermal Sciences, Graduate School of Science, Kyoto University, Noguchibaru 3088, Beppu, Oita 874-0903, Japan}

[3]{Graduate School of Life and Environmental Sciences, University of Tsukuba, Tennodai 1-1-1, Tsukuba, Ibaraki 305-8572, Japan}

[4]{Department of Natural Science, Faculty of Education, Shiga University, Hiratsu 2-5-1, Otsu, Shiga 520-0862, Japan}

Correspondence to: T. Shibata (swn05-toshibat@bep.vgs.kyoto-u.ac.jp)

Abstract

In order to refine our understanding how fluid inclusions were trapped in the host minerals, we non-destructively observed mercury inclusions (liquid Hg^0) in quartz samples using X-ray computed tomography (CT) technique. The X-ray CT apparatus can observe internal structures of the samples and give cross-sectional images from the transmission of the X-rays through the samples. From the cross-sectional images, we obtained three-dimensional spatial distributions of mercury inclusions, and quantitatively analyzed them using fractal and multifractal methods. Although the samples were from different geological settings, the resultant fractal dimensions were 1.70 and 1.71 for the San Benito and Itomuka samples, respectively. The fractal dimensions were also close to those predicted by diffusion-limited aggregation models and percolation theory, which are controlled by the irreversible kinetics. Given the fractal dimension and its implied mechanism, we conclude that the mercury-bearing fluids were not primary fluid inclusions, but migrated into the pre-existing cracks of quartz crystals by diffusion processes.

1 Introduction

Fluid inclusions in minerals record important clues to past geologic processes that the host minerals were subjected to. We can obtain information on physical and chemical factors, such as the pressure, temperature, density and composition of the fluids, from the fluid inclusions in minerals (e.g., Takeuchi, 1975; Roedder, 1984). However, studying fluid inclusions poses many difficulties for precise analysis because of the high mobility and evaporation involved. Therefore, non-destructive analytical methods, such as micro-Raman spectroscopy (Burke,

2001; Frezzotti et al., 2012), synchrotron-radiation X-ray fluorescence (SR-XRF) (Schmidt and Rickers, 2003; Tsuchiyama et al., 2009) and proton-induced X-ray emission (PIXE) (Kurosawa et al., 2003), have been developed for the chemical analysis of individual fluid inclusions in minerals. It is also necessary to observe the spatial distribution of different fluid inclusion populations within a mineral grain to establish their paragenetic succession relative to the mineral formation (i.e., primary, secondary and pseudo-secondary inclusions) (e.g., Takeuchi, 1975; Roedder, 1984). X-ray computed tomography (CT) is a non-destructive analytical method, and is one of the effective methods for observing the spatial distribution of fluid inclusions.

The X-ray CT technique, which was originally developed to obtain cross-sectional images, has recently been applied to minerals and rocks, and has opened up a new approach for resolving their internal and three-dimensional structures (Martínez et al., 2010). Although the internal structures of rocks are generally heterogeneous and complex, they have been successfully characterized using fractal geometry (Pasadas et al., 2009; Martínez et al., 2010). In particular, fractal and multifractal analysis, described by Mandelbrot (1982) and Takayasu (1986), was developed for the quantitative analysis of the patterns of irregular shapes and complicated phenomena. Fractal and multifractal analysis has been used in several geochemical studies to understand structures observed in sediments and soils, such as pore shapes and water distribution (Bird et al., 2006; Pasadas et al., 2009; Ferreiro and Vázquez, 2010; Martínez et al., 2010; Xie et al., 2010).

Here we observed mercury inclusions (liquid Hg^0) in quartz by the X-ray CT, and quantitatively analyzed their three-dimensional distribution using fractal and multifractal

methods in order to elucidate how the mercury inclusions were trapped in the host rocks. The mercury ores in this study were formed by hydrothermal activities, and mercury precipitated from the hydrothermal fluids in the late stage of ore forming processes (Peabody and Einaudy, 1992; Dunning et al., 2005). Quantitative analyses of spatial distribution of mercury inclusions should give an insight into the detailed physical behaviour of mercury during their migration and precipitation.

2 Materials and Methods

X-ray CT can be used for non-destructively analyzing the internal structures of materials. Therefore, it is suitable for samples, including fluids, that disappear if a destructive method is used. We examined a quartz crystal from San Benito, California, USA and another from Itomuka, Hokkaido, Japan (sized 2 cm × 5 cm × 7 cm and 4 cm × 5 cm × 6 cm, respectively). In these mines, native mercury (liquid Hg^0) occurs as droplets in the quartz crystals, formed by hydrothermal fluids associated with Neogene/Quaternary volcanic activities (Sugimoto et al., 1972; Harada and Haritani, 1984; Peabody and Einaudy, 1992; Dunning et al., 2005). The samples examined are idiomorphic and polycrystalline quartz, and contain visible clusters and/or films of 1–2 mm mercury inclusions.

We used a microfocus X-ray CT system (SMX-225CT; Shimazu Corp., Kyoto, Japan), which can distinguish fluid inclusion of mercury (13.59 g/cm^3) from the quartz matrix (2.65 g/cm^3) based on the difference between their densities. This apparatus forms cross-sectional images by the transmission of the X-ray through the samples. The nominal resolution of the cross-section thickness and the interval between the cross-sections were 0.120 mm and 0.073

mm, respectively. The cross-sectional images were composed of a 512 × 512 pixel array that corresponded to an area of 9.88 × 9.88 cm^2 (therefore, one pixel corresponds to an area of 0.193 × 0.193 mm^2). One of the cross-sectional images is shown in Fig. 1. The grey circle in Fig. 1a represents the field of view for the X-ray CT system, and the irregular region marked in the center of the field of view represents the quartz. The region outside of the quartz is air, containing no solid matter. The white dots represent mercury inclusions in the quartz.

The sequenced cross-sectional images were reconstructed and incorporated onto the images of each quartz crystal using the Image Processing and Analysis software in Java-ImageJ (Rasband, 1997–2011; Abramoff et al., 2004). Areas of mercury inclusions in the quartz were extracted from the images using threshold filtering. The spatial distributions of mercury inclusions were analyzed by fractal and multifractal theory.

3 Fractal and Multifractal Analysis

Fractal and multifractal behavior is common in nature, and often the spatial distributions of mercury inclusions have fractal and multifractal properties. Because a fractal typically has a self-similar structure and scale-free properties, the degree of distribution of the inclusions follows a power law in the form

$$N(r) \propto r^{-D} , \quad (1)$$

where *N(r)* is the number of boxes in a box-counting technique, *r* is the scale and *D* is the capacity (fractal) dimension. The capacity dimension, *D*, which is generally estimated using the box-counting technique, is defined by the relationship between the scaling properties of

the distribution by covering it with boxes of size, r, and counting the number of boxes containing $N(r)$, as follows:

$$D = -\lim_{r \to 0} \frac{\log N(r)}{\log r}. \quad (2)$$

Then, the capacity dimension can be approximately determined as the negative slope of $logN(r)$ versus $log\ r$. Although the capacity dimension is a fundamental and quantitative parameter of the fractal, the dimension cannot completely describe complex and heterogeneous structures. Therefore, we applied multifractal theory to analyze the spatial distribution of the mercury inclusions, as described below.

Multifractal theory can be characterized on the basis of the generalized dimensions of the q-th order moment of a distribution, D_q. The generalized dimensions, D_q, can be defined by the function

$$D_q = \lim_{r \to 0} \frac{\log \sum_i P_i(r)^q}{(q-1)\log r}, \quad (3)$$

where $P_i(r)$ is the probability of being in the i-th box, and is defined as the measure of the i-th box of its size r, when the measure of the whole space is normalized to 1 (Takayasu, 1986). The generalized dimension, D_q, can be rewritten with the singularity exponent, α, and the generalized fractal dimension, $f(\alpha)$, as the equation

$$D_q = \frac{q\alpha(q) - f(\alpha(q))}{(q-1)}. \quad (4)$$

When we can obtain the generalized dimension, D_q, from experiments, then the singularity exponent, α, and the generalized fractal dimension, $f(\alpha)$, can be estimated using the following relationships

$$\alpha(q) = \frac{d}{dq}(q-1)D_q \tag{5}$$

and

$$f(\alpha(q)) = q\alpha(q) - (q-1)D_q . \tag{6}$$

The singularity exponent, α, is characterized by scaling in the local region, and quantifies the degree of regularity in the region. The sub-sets with a local scaling exponent of α form the fractal distribution, and its fractal dimension can be viewed as the generalized fractal dimension, $f(\alpha)$. Multifractal theory allows the characterization of complex phenomena in a fully quantitative manner for both temporal and spatial variations.

4 Results and Discussion

The mercury inclusions in the host quartz crystals seemed to be clustered, and were ramified peripherally and randomly so that the clusters resembled dendritic structures. There was no natural scale length in the structures at scales much larger than the particle size, and a self-similar structure was formed. We analyzed the mercury inclusion clusters in the quartz samples using the above equations in order to understand how the inclusions were incorporated into the quartz samples. We estimated the relationship between the logarithm of the number of objects, *log N(r)*, and the logarithm of the box-size, *log r*, using the box-counting technique (Fig. 2). The capacity dimensions, D, were found to be 1.70 and 1.71 for the San Benito and Itomuka samples, respectively, from the slopes of the relationships shown in Fig. 2. The capacity dimensions generally indicate major cluster shapes, for example lines and surfaces have the values $D = 1$ and $D = 2$, respectively. The obtained dimensions

show that the mercury inclusion clusters found in the quartz samples were more complex than lines but were not entirely surfaces. Several studies have been performed using fractal geometry, which is controlled by the irreversible kinetic processes such as diffusion, aggregation and percolation (e.g., Zheng et al., 1998; Hunt and Ewing, 2009).

The San Benito and Itomuka mercury deposits occurred in hydrothermally altered rocks, which would have been formed by repeated hydrothermal activity in the Neogene/Quaternary age (Dunning et al., 2005; Sugimoto et al., 1972), and it is difficult to distinguish whether the mercury inclusions were primary, secondary or pseudo-secondary inclusions. However, as spatial distributions of mercury inclusions have fractal geometry, the mercury inclusions could not be trapped in growing crystal faces but controlled by diffusive processes. This result suggests that the fluids of mercury inclusions would be captured into quartz after its crystallization process. Hence the mercury-bearing fluids were not the primary fluid inclusions, but were trapped in cracks that already existed in the quartz samples.

In this condition, the fractal dimension of the mercury inclusion could be constrained by the available pores, pore alteration by metamorphism, and migration of mercury into the pore. These processes have been described by the diffusion-limited aggregation (DLA) and percolation mechanism, which involves Brownian particle motion (e.g., Witten and Sander, 1983; Meakin, 1985; Zheng et al., 1998; Stauffer, 1979; Hunt and Ewing, 2009). Based on the DLA models, the fractal dimension, D, is predicted to be equal to $(d^2 + 1)/(d + 1)$, where d is the spatial dimensionality (Muthukumar, 1983). For a two- and three-dimensional system D should be 5/3 (1.66) and 5/2 (2.5), respectively. Also, percolation theory shows that the fractal dimensions are 1.89 and 2.54 in two- and three-dimensional systems, respectively. Estimated

fractal dimensions of the mercury inclusions in our quartz samples from San Benito and Itomuka are similar to these obtained by DLA models and percolation theory for two-dimensional system. The mercury inclusion could be constrained by DLA models or percolation mechanism, which could lead to different structures. The DLA models and percolation mechanism result in dendritic and percolation structures, respectively (e.g., Zheng et al., 1998; Hunt and Ewing, 2009). Consequently, mercury inclusions were ramified like a dendritic structure, but not like a loop structure as illustrated in Fig. 3. Therefore, we assume that the mercury inclusions could migrate into the quartz by the DLA models rather than by percolation mechanism.

Multifractal analysis allowed us to examine the complex signature of the mercury inclusion clusters more quantitatively. We obtained three sets of multifractal parameters, α, $f(\alpha)$ and D_q. Figure 4 shows multifractal spectra in which the generalized fractal dimensions, $f(\alpha)$, are plotted against the singularity exponent, α. Multifractal spectra generally show parabolic curves that are concave downwards, and the curve maxima occur at $q = 0$, at which point $f(\alpha)$ in the San Benito and Itomuka samples corresponded to the capacity dimensions of 1.70 and 1.71, respectively. The parabola of both samples had similar curves, but the width of the parabola was larger for the San Benito sample than for the Itomuka sample. The San Benito sample had more fractal structure patterns than the Itomuka sample, because wider curves reflect more heterogeneous structures in the mercury inclusion distributions.

Figure 4 shows the difference between the fractal dimension distributions in the samples, and the relationships between the generalized dimensions, D_q, and the order moments, q. In general, D_q dimensions increase with decreasing q moments. In Fig. 5, the curves for both

quartz samples are similar. The q moments are interpreted as a parameter of the inclusion distribution probability densities, i.e., low-q implies a low distribution density and high-q implies a high density. The D_q dimensions at low-q moments in the samples were 2.3–2.7, indicating that the distribution of surface and spatial structures were scarce. However, the D_q dimensions at high-q moments were 1.0–1.3, indicating that linear configurations were common. This implies that mercury-bearing fluids migrated linearly into the quartz sample cracks and then expanded to form surface plane and spatial figurations.

5 Conclusions

We analyzed mercury inclusions in quartz samples using in situ X-ray computed tomography (CT). The X-ray CT apparatus allows the internal structures of the quartz samples to be analyzed non-destructively, and therefore, mercury inclusions are to be retained in the quartz throughout the experiment. We performed X-ray CT measurements on two quartz samples, one from San Benito, California, USA and one from Itomuka, Hokkaido, Japan, both of which contain visible mercury inclusions. We obtained the spatial distributions of the mercury inclusions based on sequenced X-ray cross-sectional images. Spatial distributions can be explored quantitatively using fractal and multifractal theory. We showed the fractal dimensions, α–$f(\alpha)$, multifractal spectra and the relationship between q and D_q. The mercury inclusions trapped in the quartz samples had similar distribution signatures, even though the quartz samples were from different geological settings. In addition, the fractal dimensions were close to those obtained by diffusion-limited aggregation DLA models and percolation theory for two-dimensional system. The similar mercury inclusion signatures correspond to

the samples being formed during a process of diffusion into pre-existing cracks in the quartz. After the formation of crystalline quartz, the mercury-bearing fluids probably migrated into pre-existing cracks in the quartz crystals, and native mercury was lodged in the cavities.

Author contributions

T.S. designed the study, T.M. performed the X-ray CT measurements and T.E. prepared samples. T.M. and T.E. gave technical supports and conceptual advice, and T.S. prepared the manuscript with contributions from all co-authors.

Acknowledgements

This study was financially supported in part by Grant-in-Aid for Scientific Research from the Ministry of Education, Science and Culture, Japan (18251002, PD20–1531, 23840049 and 24101010) and the Fukada Geological Institute (2011#7). The authors wish to thank the Editor A. G. Hunt, reviewer R. P. Ewing and S. Tarafdar for helpful suggestions in the preparation of this manuscript.

References

Abramoff , M. D., Magalhaes, P. J., and Ram, S. J.: Image processing with ImageJ, Biophotonics International, 11, 36–42, 2004.

Bird, N., Díaz, M. C., Saa, A., and Tarquis, A. M.: Fractal and multifractal analysis of pore-scale images of soil, J. Hydrol., 322, 211–219, 2006.

Burke, E. A. J.: Raman microspectrometry of fluid inclusions, Lithos, 55, 139–158, 2001.

Dunning, G. E., Hadley, T. A., Magnasco, J., Christy, A. G., and Cooper Jr., J. F.: The clear Creek mine, San Benito county, California: a unique mercury locality, Mineral. Rec., 36, 337–363, 2005.

Ferreiro, J. P. and Vázquez, E. V.: Multifractal analysis of Hg pore size distributions in soils with contrasting structural stability, Geoderma, 160, 64–73, 2010.

Frezzotti, M. L., Tecce, F., and Casagli, A.: Raman spectrometry for fluid inclusion analysis, J. Geochem. Explor., 122, 1–20, 2012.

Harada, J. and Haritani, Y.: Minerals in Hokkaido, Geological Survey of Hokkaido, Sapporo, 1984.

Hunt, A. and Ewing, R.: Percolation Theory for Flow in Porous Media, 2nd edn., Lecture Notes in Physics 711, Springer, Berlin, 2009.

Kurosawa, M., Shimano, S., Ishii, S., Shima, K., and Kato, T.: Quantitative trace element analysis of single fluid inclusions by proton-induced X-ray emission (PIXE): application to fluid inclusions in hydrothermal quartz, Geochim. Cosmochim. Ac., 67, 4337–4352, 2003.

Mandelbrot, B. B.: The Fractal Geometry of Nature, W. H. Freeman, San Francisco, 1982.

Martínez, F. S. J., Martín, M. A., Caniego, F. J., Tuller, M., Guber, A., Pachepsky, Y., and Carcía-Gutiérrez, C.: Multifractal analysis of discretized X-ray CT images for the characterization of soil macropore structures, Geoderma, 156, 32–42, 2010.

Meakin, P.: The structure of two-dimensionalWitten-Sander aggregates, J. Phys. A-Math. Gen., 18, L661–L666, 1985.

Muthukumar, M.: Mean-field theory for diff usion-limited cluster formation, Phys. Rev. Lett., 50, 839–842, 1983.

Peabody, C. E. and Einaudy, M.: Origin of petroleum and mercury in the Culver-Baer cinnabar deposit, Mayacmas district, California, Econ. Geol., 87, 1078–1103, 1992.

Posadas, A., Quiroz, R., Tannús, A., Crestana, S., and Vaz, C. M.: Characterizing water fingering phenomena in soils using magnetic resonance imaging and multifractal theory, Nonlin. Processes Geophys., 16, 159–168, doi:10.5194/npg-16-159-2009, 2009.

Rasband, W. A.: ImageJ, US National Institutes of Health, Bethesda, Maryland, USA, available at: imagej.nih.gov/ij/, last access: July 2014, 1997–2011.

Roedder, E.: Fluid inclusions, in: Reviews in Mineralogy, Mineralogical Society of America, 12, 1–646, 1984.

Schmidt, C. and Rickers, K.: In-situ determination of mineral solubilities in fluids using a hydrothermal diamond-anvil cell and SR-XRF: solubility of AgCl in water, Am. Mineral., 88, 288–292, 2003.

Stauff er, D.: Scaling theory of percolation clusters, Phys. Rep., 54, 1–74, 1979.

Sugimoto, R., Fujiwara, T., and Futamase, K.: Mercury ore deposits of Itomuka district, Abashiri province, Hokkaido, Report of the Geological Survey of Hokkaido, 45, 1–23, 1972.

Takayasu, H.: Fractals, Asakura-Shoten, Tokyo, 1986.

Takeuchi, S.: Basic knowledge on studies of fluid inclusions minerals 1: Historical review, classification and formation of fluid inclusions, Journal of the Gemmological Society of Japan, 2, 25–33, 1975.

Tsuchiyama, A., Nakamura, T., Okazaki, T., Uesugi, K., Nakano, T., Sakamoto, K., Akaki, T., Iida, Y., Kadono, T., Jogo, K., and Suzuki, Y.: Three-dimensional structures and elemental distributions of stardust impact tracks using synchrotron microtomography and X-ray fluorescence analysis, Meteorit. Planet. Sci., 44, 1203–1224, 2009.

Witten, T. A. and Sander, L. M.: Diff usion-limited aggregation, Phys. Rev. B, 27, 5686–5697, 1983.

Xie, S., Cheng, Q., Xing, X., Bao, Z., and Chen, Z.: Geochemical multifractal distribution patterns in sediments from ordered streams, Geoderma, 160, 36–46, 2010.

Zheng, D. W., Wen, W., and Tu, K. N.: Reactive wetting- and dewetting-induced diffusion-limited aggregation, Phys. Rev. B, 57, R3719–R3722, 1998.

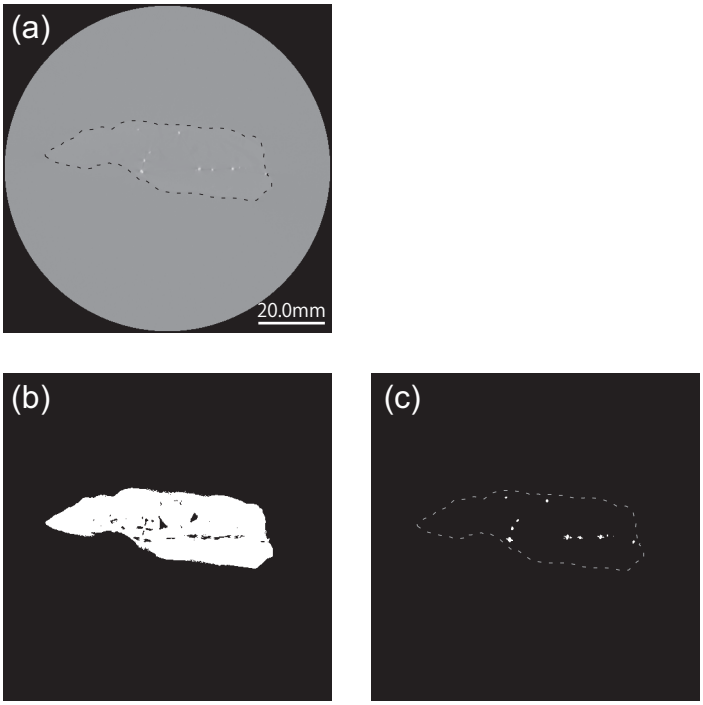

Fig. 1. Two-dimensional (2-D) slice image of the San Benito quartz sample obtained with a microfocus X-ray CT system. **(a)** Original grayscale image. The circular dark gray region is the measurable area, the irregular central region is the quartz sample, and the white points are mercury inclusions; **(b)** Binarized image of the quartz crystal; and **(c)** Binarized image of the mercury inclusions. The quartz area is edged with a dotted line.

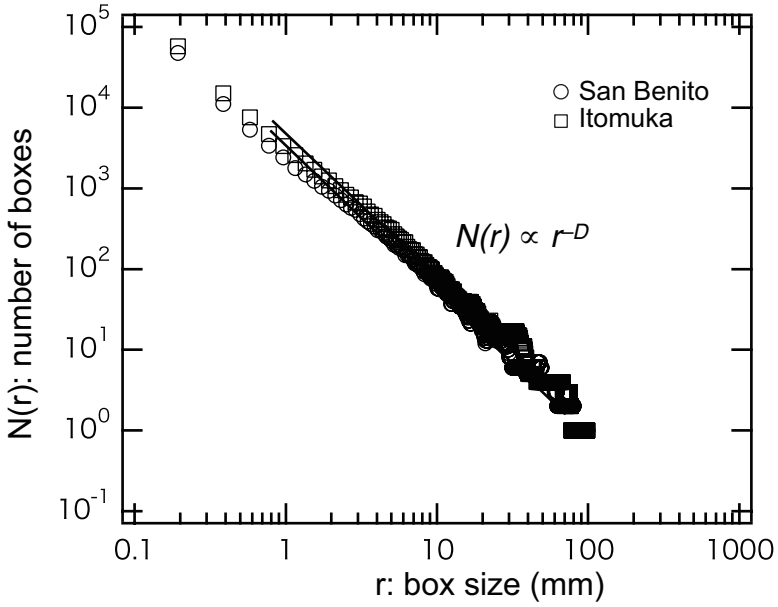

Fig. 2. Box counting plot for mercury inclusions in the San Benito and Itomuka quartz samples. To obtain the capacity dimensions, D, only the middle portions of the sequence, from four times the length of the minimal box size to 9/10 of the length of the maximal box size, were analysed to avoid edge effects.

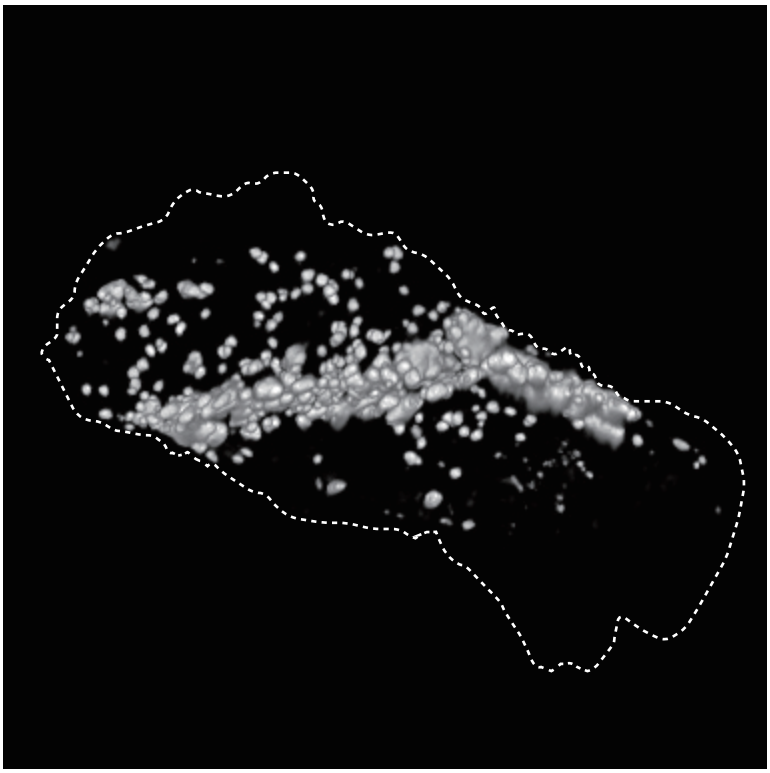

Fig. 3. Distribution image of the mercury inclusions in the San Benito quartz sample obtained with a micro-focus X-ray CT system. Mercury inclusions are lighten and the quartz area is edged with a dotted line.

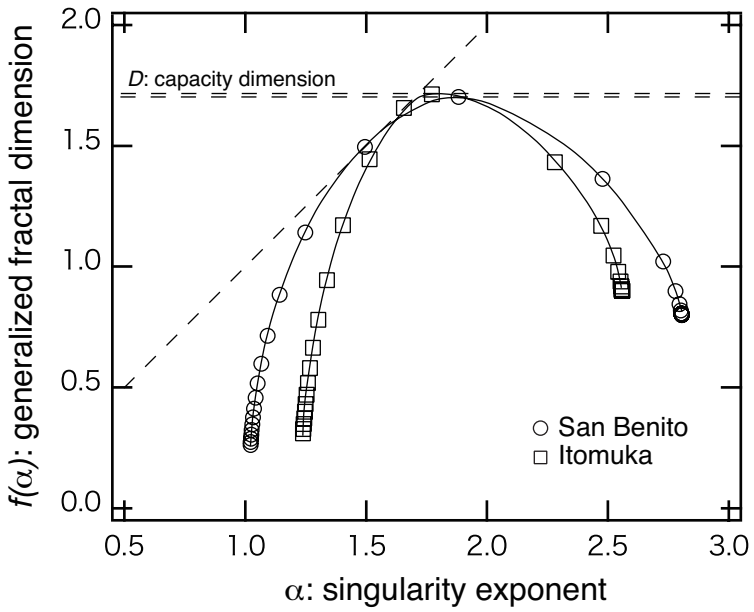

Fig. 4. Multifractal spectrum for the mercury inclusions in the San Benito and Itomuka quartz samples. The spectrum is the shape of a downward concave parabola. A wide opening parabola indicates heterogeneous distribution structures in the mercury inclusions. The opening size of parabola in the San Benito sample is larger than that of Itomuka sample, suggesting that mercury inclusions in the San Benito distribute the more heterogeneous than those in Itomuka.

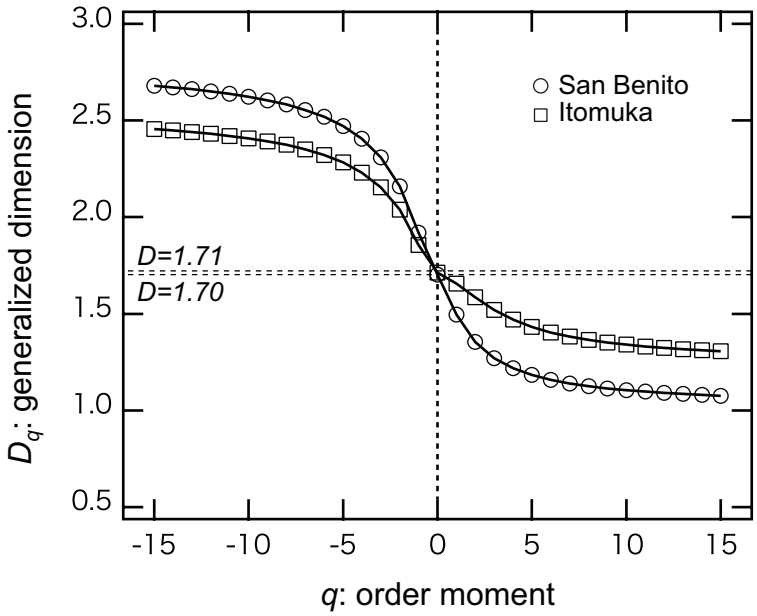

Fig. 5. Generalized dimension, D_q, versus the order moment, q, from $q = -15$ to $q = +15$ for the mercury inclusion distribution in the San Benito and Itomuka quartz samples. The q moment is a measure of the probability density, low-q is low-density and high-q is high-density. The generalized dimension, D_q, indicates the geometrical shape of the mercury inclusion at the q-density.